Unveiling the atomistic and electronic structure of NiII–NO adduct in MOF-based catalyst by EPR spectroscopy and quantum chemical modelling

*Kavipriya Thangavel,[1,2‡] Paolo Cleto Bruzzese,[1,3‡] Matthias Mendt,[1] Andrea Folli,[2] Katharina Knippen,[4] Dirk Volkmer,[4] Damien M. Murphy,[2] Andreas Pöppl[1] ***

Felix Bloch Institute for Solid State Physics, Leipzig University, Linnéstraße 5, 04103 Leipzig, Germany
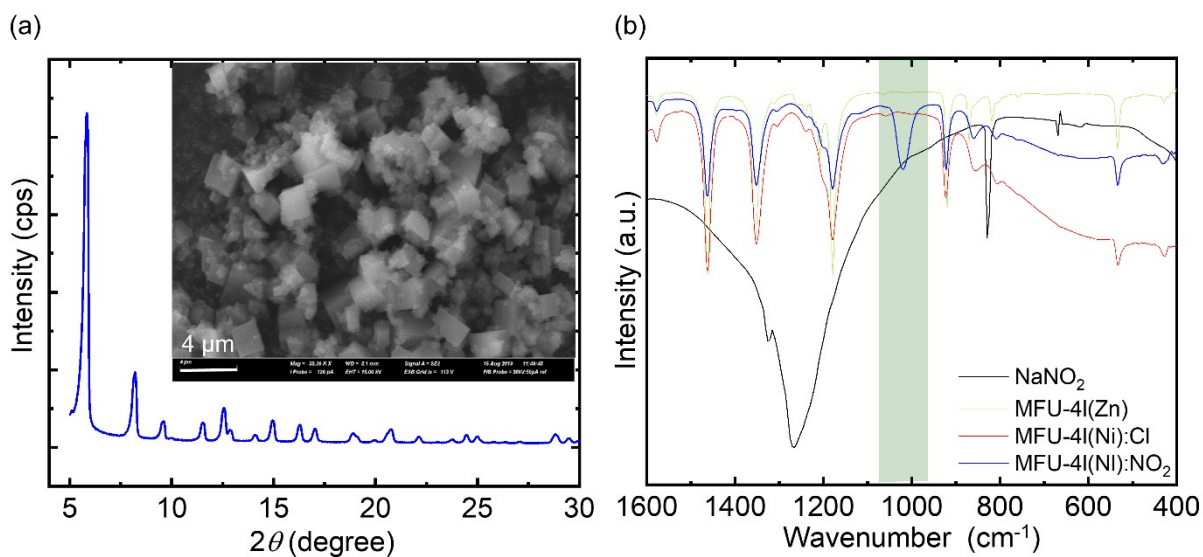
School of Chemistry, Main building, Cardiff University, Cardiff CF10 3AT, UK

Institute of Physics, Solid State and Materials Chemistry, University of Augsburg, Universitätstraße 1, D-86159 Augsburg, Germany

Table of contents

1. Structural characterizations

Figure S1. (a) PXRD and SEM image (inset: scale bar - 4 μm) of Ni-MFU-4l:NO$_2$ and (b) IR spectra comparison of various MFU-4l materials

IR bands of Ni-MFU-4l-NO$_2$ (cm^{-1}): 1625 (w), 1575 (w), 1461 (vs), 1351 (vs), 1210 (sh), 1183 (vs), 1025 (w), 922 (s), 867 (m), 817 (m), 535 (m), 430 (w) matches with the reported values,[1] where, w, s, m ,vs, sh indicates weak, strong, medium, very strong and shoulder, respectively.

2. Simulation of Q- and W- band EPR spectra of Ni^{II} in Ni-MFU-4l-NO$_2$

a)

b)
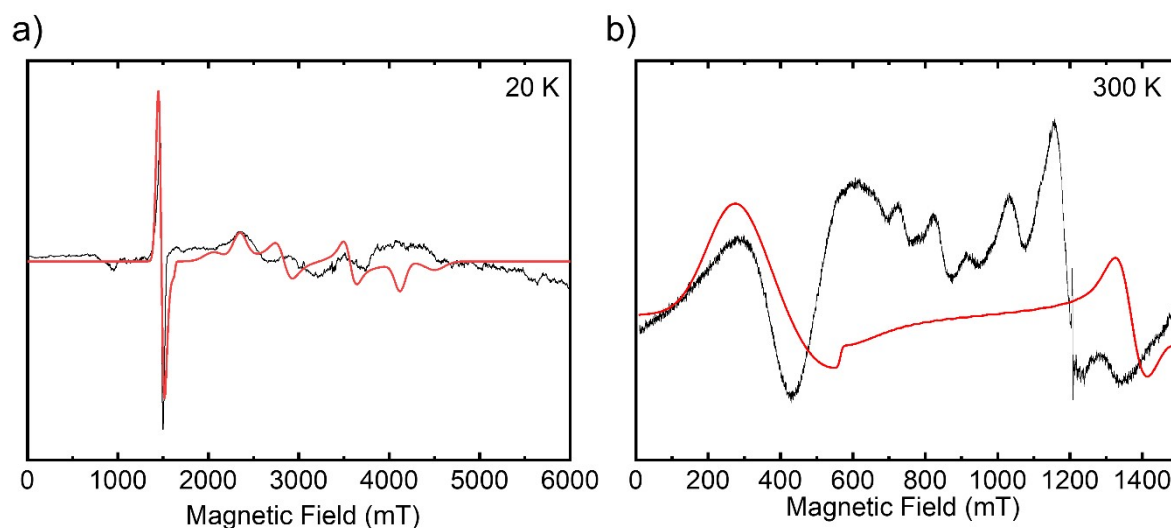
Figure S2. (a) W-band and (b) Q-band EPR spectra (black) and simulation (red) of the spin $S = 1$ of Ni^{II} in Ni-MFU-4l-NO$_2$ with the spin Hamiltonian parameters $g_{xx} = 2.050(5)$, $g_{yy} = 2.055(6)$, $g_{xx} = 2.060(5)$, $D = 35.5(5)$ GHz and $E = 0.5$ GHz. (the extra signals of Q-band data are from the EPR cavity and the radical from the MOF sample.)

a)

b)
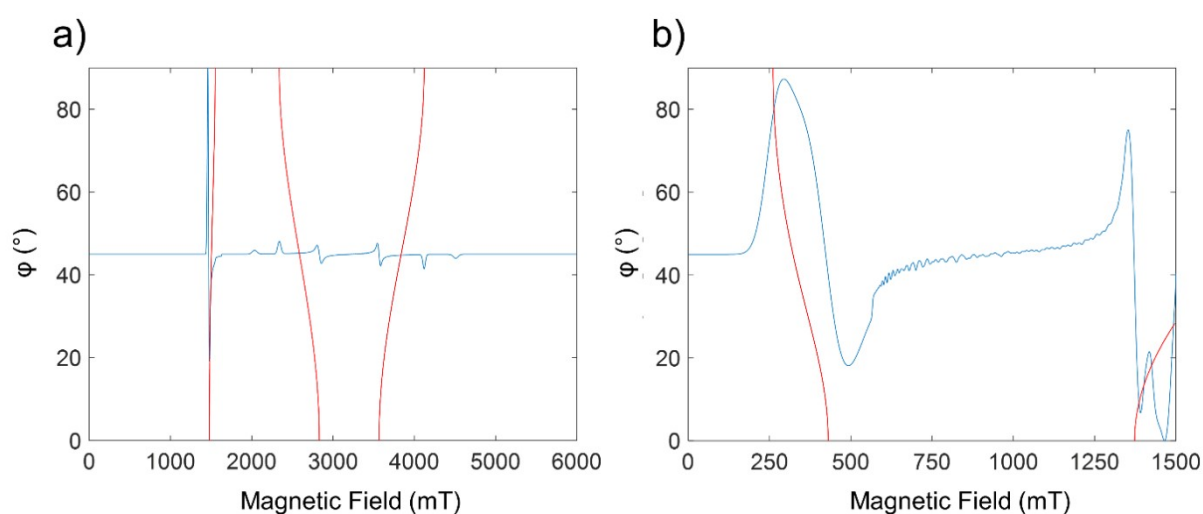
Figure S3. Angular dependent road map for the $S = 1$ Ni^{II} species at (a) W-band and (b) Q-band frequency (Blue - simulated EPR spectra with spin Hamiltonian parameters $g_{iso} = 2.05$, $D = 35500$ MHz and $E = 5000$ MHz; Red – Road map of the expected spectral position).

3. Geometry optimization of Ni-MFU-4l-NO$_2$ and Ni-MFU-4l-Cl

a)

b)
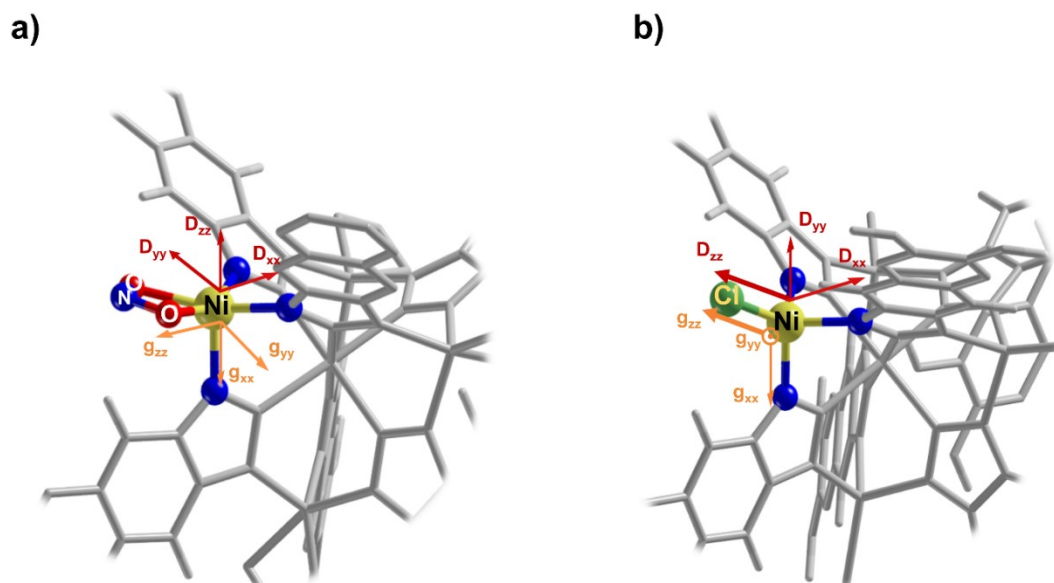
Figure S4. Geometry optimized periodic structures at B3LYP-D3/pob-TZVP-rev2 of (a) Ni-MFU-4l-NO$_2$ and (b) Ni-MFU-4l-Cl. The computed *g*- and *D*-frames are also reported. Nitrogen and oxygen atoms are shown in blue and red, respectively. The other atoms are labelled in the figures.

4. Temperature dependent CW X-band data of NO adsorbed Ni-MFU-4l-NO₂

a)

b)
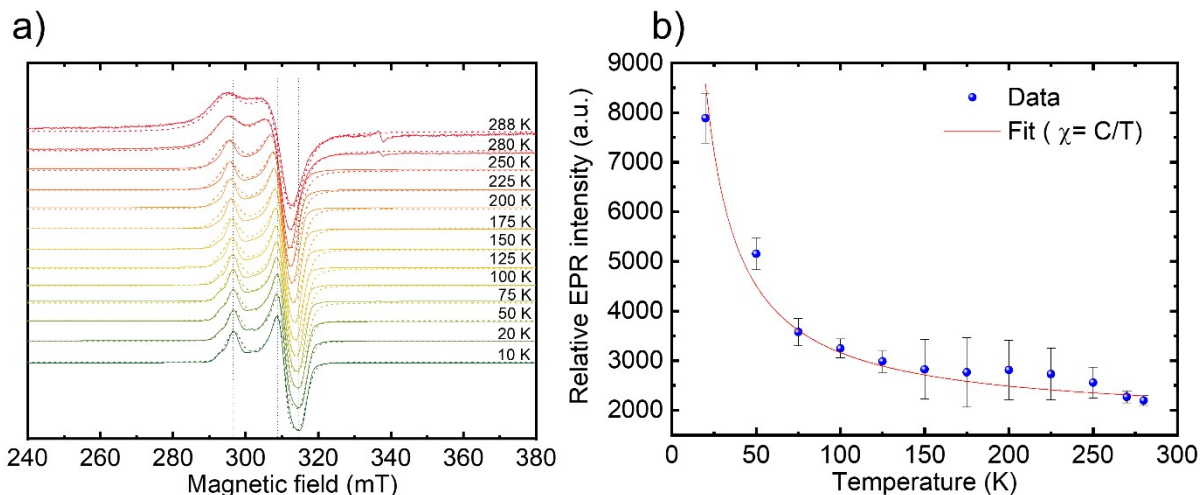
Figure S5. (a) Temperature-dependent X-band EPR spectra of NO adsorbed over Ni-MFU-4l-NO$_2$ ranging from temperature 10 K to 288 K (solid line – experimental data and dotted line – simulation of the sum of two different species A and B) and (b) Intensity corresponds to magnetic susceptibility as a function of temperature, extracted from double integration of full range temperature dependent EPR data (fit – red: paramagnetic susceptibility fit). The small signal around ~340 mT corresponds to the radical.

Table S1. Experimental spin Hamiltonian parameters for the Ni^{II}-NO adduct in Ni-MFU-4l-NO$_2$ of species A recorded at several temperatures. (Gaussian (ΔB^{pp}_G)and Lorentzian (ΔB^{pp}_L) broadening)

T (K)	g_{xx}	g_{yy}	g_{zz}	ΔB^{pp}_G (mT)	ΔB^{pp}_L (mT)
10	2.1358(5)	2.1672(5)	2.2705(5)	2.1(1)	0.8(1)
20	2.1358(5)	2.1672(5)	2.2705(5)	2.1(1)	0.8(1)
50	2.1358(4)	2.1672(5)	2.2705(5)	2.1(1)	0.8(1)
75	2.1358(4)	2.1672(5)	2.2720(5)	2.1(1)	1.1(1)
100	2.1376(6)	2.1672(6)	2.2727(6)	2.1(1)	1.1(1)
125	2.1385(5)	2.1685(7)	2.2745(4)	2.1(1)	1.20(7)
150	2.1392(8)	2.1690(7)	2.2757(6)	2.1(1)	1.35(6)
175	2.1410(6)	2.1692(9)	2.2766(5)	2.1(1)	1.35(10)
200	2.1446(6)	2.1710(7)	2.2780(8)	2.1(1)	1.40(7)
225	2.1498(8)	2.1725(10)	2.2788(8)	2.2(2)	1.45(10)
250	2.1518(9)	2.1740(8)	2.2800(9)	2.3(3)	2.0(1)
280	2.1545(4)	2.1745(6)	2.2820(9)	2.3(4)	3.3(2)
288	2.1545(7)	2.1745(5)	2.2850(6)	2.5(5)	4.20(10)
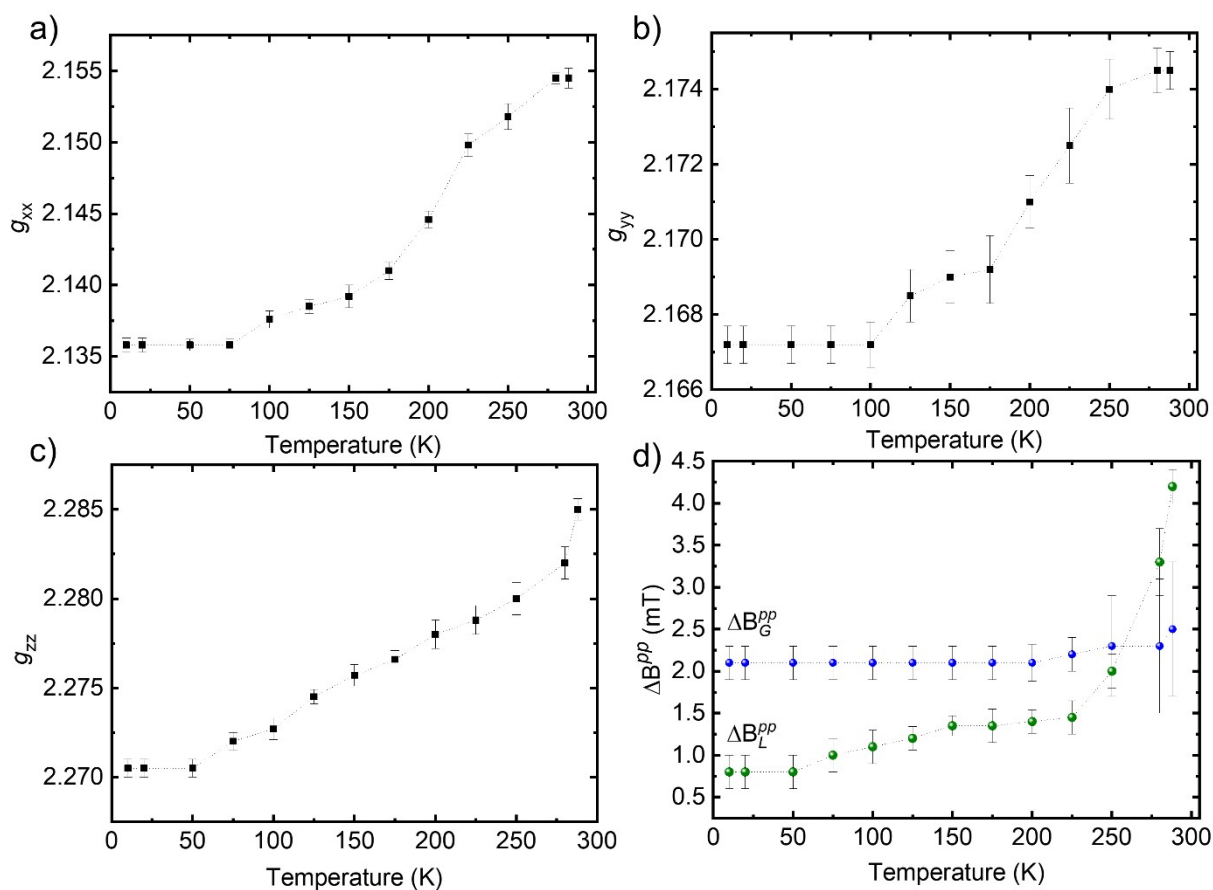
Figure S6. The temperature-dependent trend of **g**-tensor parameters (a) g_{xx} , (b) g_{yy} , (c) g_{zz} and (d) Gaussian (blue) and Lorentzian (black) linewidth for NO adsorbed Ni-MFU-4l-NO$_2$ system (species A).
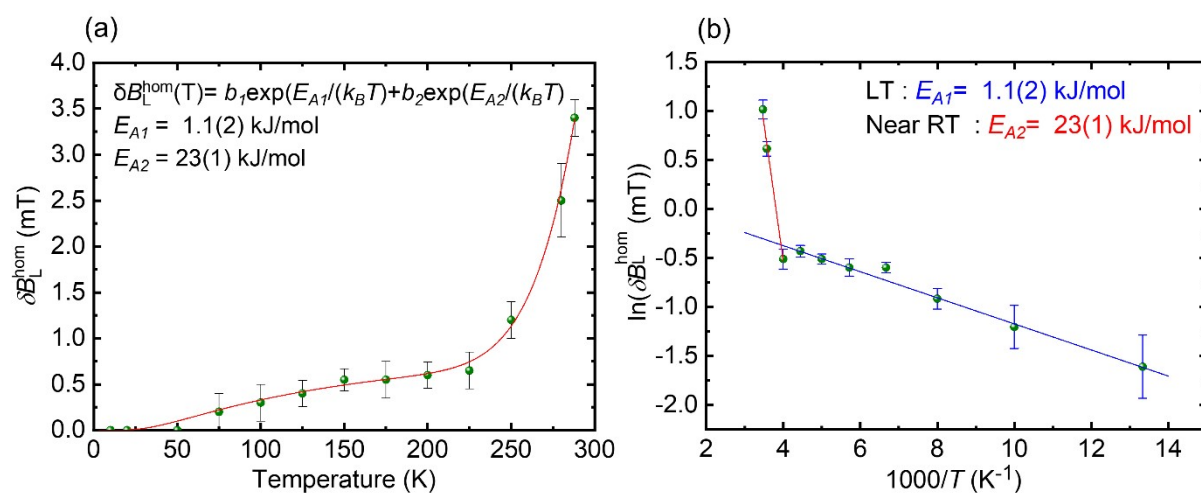
Figure S7. Arrhenius plot of the homogeneous (a) EPR linewidths, $\delta B\,^{hom}_{L}$ and (b) ln $(\delta B\,^{hom}_{L})$ of Ni^{II}-NO adduct in Ni-MFU-4l-NO$_2$. The activation energies were found to be E_{A1} = 1.1(2) kJ/mol for the lower temperature range (75 K – 250 K) and E_{A2} = 23(1) kJ/mol for the higher temperature range (250 K – 288 K). $\delta B\,^{hom}_{L}$ (T) = $\delta^{total} B_i$ (T) − $\delta^{total} B_i$ (50 K)

All three principal values g_{ii} of the **g**-tensor of the Ni^{II}-NO species A in Ni-MFU-4l-NO$_2$ as determined by spectral simulations (Table S1) increase with rising temperature (Fig. S6a-c). Such temperature-dependent g-tensor but also hfi tensor parameters of paramagnetic transition metal ions or adsorption complexes in solids can be caused by motional effects of these species either related to lattice vibrations or internal motional processes. However, these motional processes result in a partial averaging of the principal values.[2,3] In the case of Ni-MFU-4l-NO$_2$, all three parameters g_{ii} of the Ni^{II}-NO adsorption complex increase with temperature, and no averaging of the principal values is observed. Therefore, we rather suggest that temperature-dependent enhancements of the mean values of the nitrogen–metal ion bond length in the nickel coordination might lead to the observed temperature dependence of the g_{ii} parameters. These would result in smaller energy splitting Δ_j between the $\left(3d_{x^2-y^2}\right)$ ground state and the excited states giving rise to an increase of all three parameters g_{ii} (eq. 3).

The spectral simulations also revealed that the total linewidth of the EPR signal of the Ni^{II}-NO species A in Ni-MFU-4l-NO$_2$ is composed of a Gaussian ΔB_G^{pp} and a Lorentzian ΔB_L^{pp} linewidth contribution (**Table S1**) (**Figure S6d**). Whereas the Gaussian linewidth ΔB_G^{pp}, usually associated with an inhomogeneous line broadening, appears to be temperature independent within the error margin of the simulations, the Lorentzian linewidth contribution indicating homogeneous broadening increases at a temperature above $T > 50$ K. For the later, we calculated the temperature-dependent contribution $\delta B_L^{hom}(T)$ to the total Loentzian line broadening according to

$$\delta B_L^{hom}(T) = \Delta B_L^{pp}(T) - \Delta B_L^{pp}(T = 50\ K) \qquad (S1)$$

presented in **Figure S7**. $\delta B_L^{hom}(T)$ seems to be determined by two temperature-dependent processes, both following approximately an Arrhenius-type behavior

$$\delta B_L^{hom}(T) = b_1 \exp\left(-\frac{E_{A1}}{k_B T}\right) + b_2 \exp\left(-\frac{E_{A2}}{k_B T}\right) \qquad (S2)$$

with the absolute values of E_{A1} = 1.1(2) kJ/mol (11(2) meV), E_{A2} = 23(1) kJ/mol (240(35) meV), b$_1$ = 1 mT, b$_2$ = 42974 mT, and the Boltzmann constant k_B. Elucidation of the exact nature of the two motional processes is beyond the scope of this work, but we may assume that they might be related to spin-lattice relaxation (E_{A1}) and starting desorption processes of NO at elevated temperatures (E_{A2}).

5. Optimized structure of Ni^{II}-NO versus Zn^{II}-NO adsorption complexes in Ni-MFU-4l-NO$_2$

a)

b)
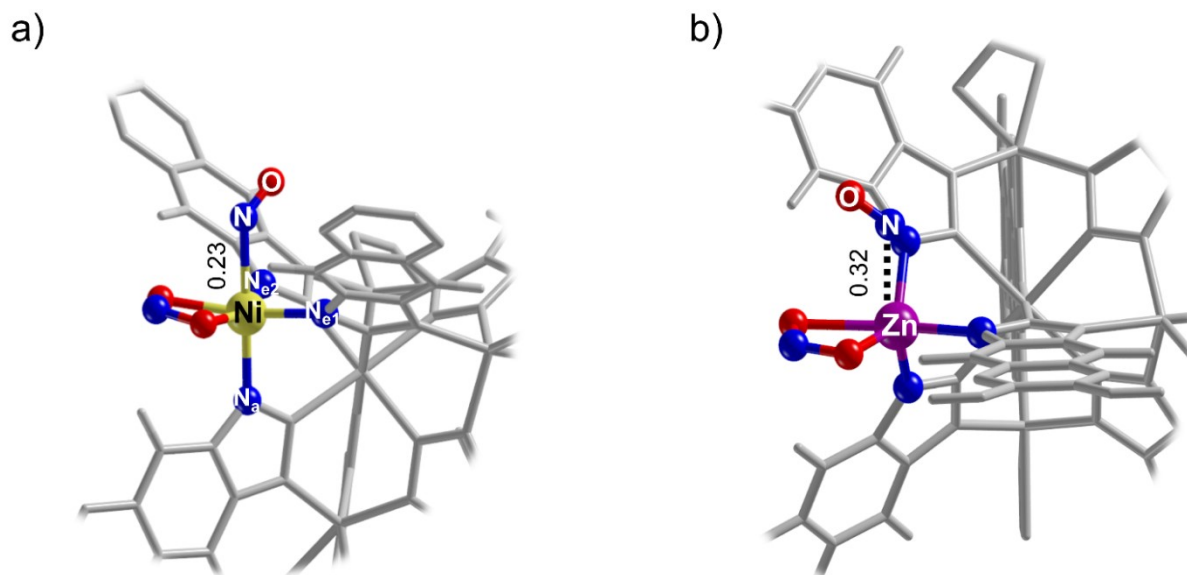
Figure S8. Atomistic structure of NO adsorbed on Ni-MFU-4l-NO$_2$. (a) Ni^{II}-NO and (b) Zn^{II}-NO binding sites. The metal-nitrosyl bond distances are reported in nm together with the computed relative electronic energy for the two configurations.

6. Experimental and simulated ^{14}N ENDOR spectra of the Ni^{II}-NO adsorption complex in Ni-MFU-4l-NO$_2$
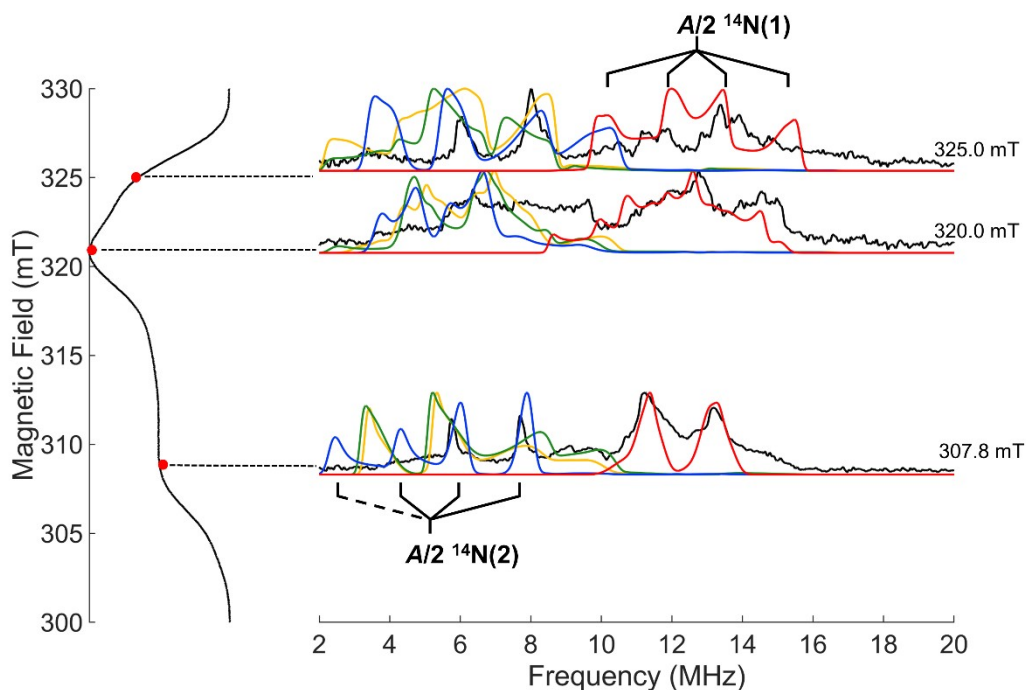
Figure S9. X-band ^{14}N ENDOR spectra simulation of the Ni^{II}-NO species in Ni-MFU-4l-NO$_2$ highlighting the contribution of each ^{14}N species. The black lines are the experimental spectra. The ESE spectrum with the corresponding field position sampled is plotted on the left. The blue, green and yellow lines represent the simulation obtained with the spin Hamiltonian of ^{14}N(2) by using the orientation computed from N_{f1}, N_{f2} and N_{f3}, respectively. The red line is obtained by using the spin Hamiltonian parameters of ^{14}N(1).

Table S2. Computed Euler rotation of hyperfine (α, β, γ) and quadrupolar tensors (α', β', γ') to the g-tensor. First rotation by α around z; second rotation by β around y'; third rotation by γ around z". A positive sign corresponds to a clockwise rotation, a negative sign to a counterclockwise rotation. The tensor values (calculated at CASSCF level of theory) are in MHz, while angles (calculated at DFT level of theory) are in degrees.
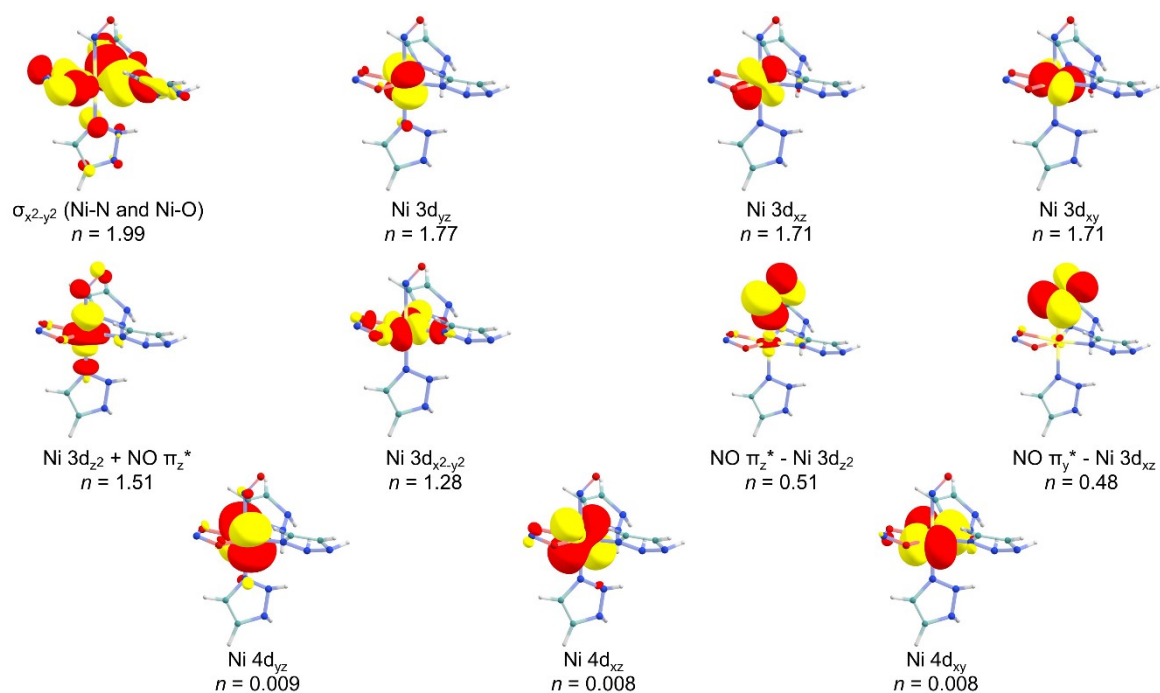
g-tensor				^{14}N A-tensor								^{14}N Q-tensor		
				A_x	A_y	A_z	α	β	γ			α'	β'	γ'
			N_{NO}	-14.8	-14.3	-24.9	79.0	11.7	-106.3	5.0	0.3	140.0	12.9	-98.9
			N_{f1}	8.4	8.6	12.7	-136.7	50.4	114.7	4.7	0.5	-140.0	49.2	132.3
2.226	2.255	2.276	N_{f2}	8.1	8.3	12.4	42.7	30.8	-56.4	4.6	0.4	21.1	18.7	-41.5
			N_{f3}	6.8	6.9	10.4	-120.7	13.2	138.6	4.3	0.4	-146.7	19.6	154.4
			N_s	0.4	0.3	1.2	-48.4	14.6	53.1	5.8	0.5	84.2	39.3	-80.2

# 7. Computed and experimental IR spectra for Ni-MFU-4l-NO$_2$ and Ni-MFU-4l-Cl
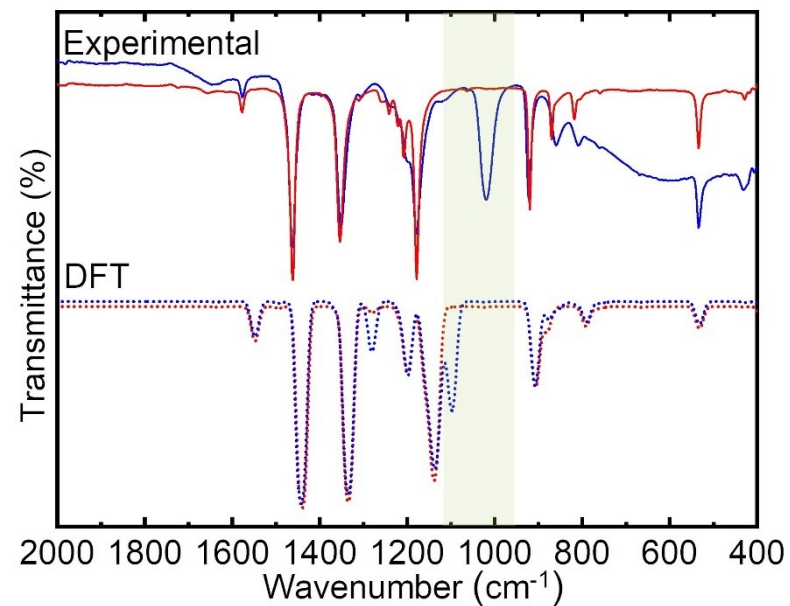
Figure S10. Calculated (at B3LYP-D3(ABC)/pob-TZVP-rev2 level of theory) and experimental comparison of IR spectra for the Ni-MFU-4l-NO$_2$ (blue spectra) and Ni-MFU-4l-Cl (red spectra) samples.

8. Contour plots of natural CASSCF(11e,11o) orbitals of the Ni^{II}-NO adsorption complex

$\sigma_{x^2-y^2}$ (Ni-N and Ni-O)
n = 1.99

Ni 3d$_{yz}$
n = 1.77

Ni 3d$_{xz}$
n = 1.71

Ni 3d$_{xy}$
n = 1.71

Ni 3d$_{z^2}$ + NO π_z*
n = 1.51

Ni 3d$_{x^2-y^2}$
n = 1.28

NO π_z* - Ni 3d$_{z^2}$
n = 0.51

NO π_y* - Ni 3d$_{xz}$
n = 0.48

Ni 4d$_{yz}$
n = 0.009

Ni 4d$_{xz}$
n = 0.008

Ni 4d$_{xy}$
n = 0.008

Figure S11. Contour plots (±0.03 a.u.) of natural CASSCF(11e,11o) orbitals with indicated qualitative character and fractional occupation number (n). N, O, Ni, C, Zn and H atoms are reported in blue, red, yellow, green, violet and white, respectively.

9. Comparison of EPR spectra with different amounts of NO loading over Ni-MFU-4l-NO$_2$
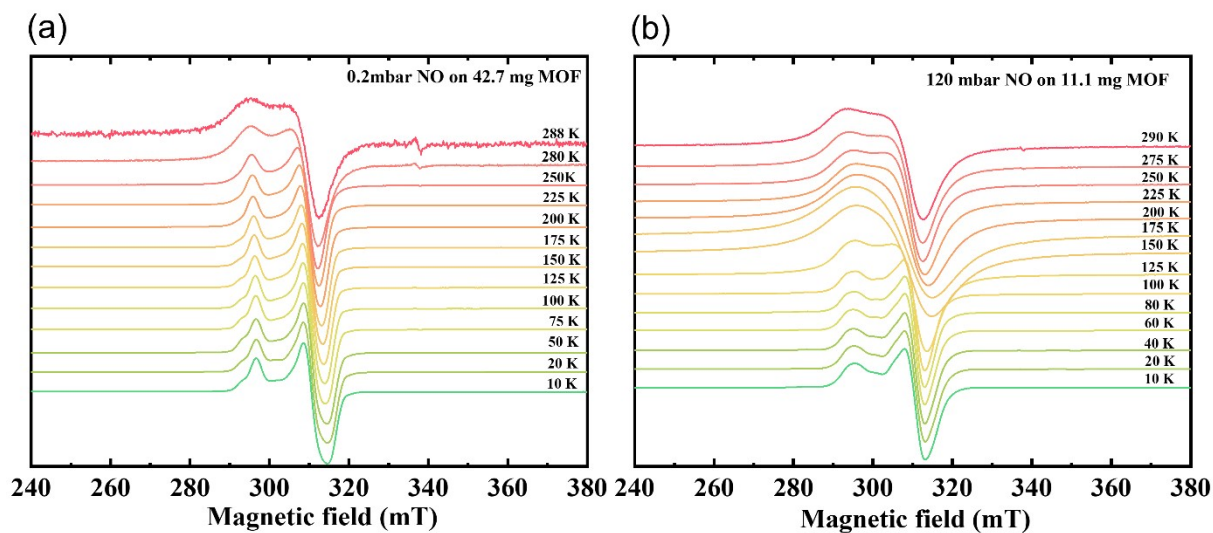
Figure S12. Temperature-dependent X-band EPR spectra of NO adsorbed over Ni-MFU-4l-NO$_2$ (a) with 0.2 and (b) 120 mbar

Supplementary References

1. D. Denysenko and D. Volkmer, *Faraday Tras.*, 2017, **201**, 101.

2. A. Gutsze, M. Plato, H.G. Karge and F. Witzel, *Faraday Tras.*, 1996, **92**(13), 2495.

3. T. Rudolf, A. Pöppl, W. Brunner and D. Michel, *Magn. Reson. Chem.*, 1999, **37**(13), S93-S99.